ARTICLE

A Simple Model for the Afternoon and Early Evening Decay of Convective Turbulence Over Different Land Surfaces

Daniel F. Nadeau · Eric R. Pardyjak · Chad W. Higgins · Harinda Joseph S. Fernando · Marc B. Parlange

Abstract   A simple model to study the decay of turbulent kinetic energy (TKE) in the convective surface layer is presented. In this model, the TKE is dependent upon two terms, the turbulent dissipation rate and the surface buoyancy fluctuations. The time evolution of the surface sensible heat flux is modelled based on fitting functions of actual measurements from the LITFASS-2003 field campaign. These fitting functions carry an amplitude and a time scale. With this approach, the sensible heat flux can be estimated without having to solve the entire surface energy balance. The period of interest covers two characteristic transition sub-periods involved in the decay of convective boundary-layer turbulence. The first sub-period is the afternoon transition, when the sensible heat flux starts to decrease in response to the reduction in solar radiation. It is typically associated with a decay rate of TKE of approximately t^{-2} (t is time following the start of the decay) after several convective eddy turnover times. The early evening transition is the second sub-period, typically just before sunset when the surface sensible heat flux becomes negative. This sub-period is characterized by an abrupt decay in TKE associated with the rapid collapse of turbulence. Overall, the results presented show a significant improvement of the modelled TKE decay when compared to the often applied assumption of a sensible heat flux decreasing instantaneously or with a very short forcing time scale. In addition, for atmospheric modelling studies, it is suggested that the afternoon and early evening decay of sensible heat flux be modelled as a complementary error function.

D. F. Nadeau · C. W. Higgins · M. B. Parlange
School of Architecture, Civil and Environmental Engineering, École Polytechnique Fédérale de Lausanne, Station 2, 1015 Lausanne, Switzerland

E. R. Pardyjak (✉)
Department of Mechanical Engineering, University of Utah, 50 S. Central Campus Dr., Salt Lake City, UT 84112, USA
e-mail: pardyjak@eng.utah.edu

H. J. S. Fernando
Department of Civil Engineering and Geological Sciences, University of Notre Dame, Notre Dame, IN 46556, USA

1 Introduction

The daytime atmospheric boundary layer (ABL) is typically characterized by unstable stratification, turbulent mixing of momentum, heat, scalars and buoyancy-driven eddies. These large eddies are generated by a strong surface heat flux (Emanuel 1994). The typical nighttime boundary layer is very different. Stable stratification associated with surface inversions tends to suppress vertical motions generated by mechanical turbulence, thus leading to much lower turbulence levels than typically observed during daytime (Fernando 2002; Cheng et al. 2005; Bou-Zeid et al. 2010).

The physics associated with the transition from the convective to the stable regimes of the ABL are less well studied and understood than other time periods (e.g. fully convective or strongly stable boundary layers). Hence, this decay period is very challenging to model and has profound implications on the dispersion of pollutants during nighttime. There has been an increasing interest in this transition period in recent years (Grant 1997; Sorbjan 1997, 2007; Goulart et al. 2003, 2010; Beare et al. 2006; Kleissl et al. 2006; Pino et al. 2006), with analyses involving numerical simulations, laboratory work and field experiments.

Much of the current understanding regarding the decay of the convective boundary layer over flat homogeneous terrain is a result of large-eddy simulation (LES) studies. The pioneering work of Nieuwstadt and Brost (1986) introduced the important scaling parameters for the case in which the surface heat flux was instantaneously removed. About a decade later, Sorbjan (1997) added the complexity of a short forcing time scale. His LES study investigated the effect of a progressive decrease of the surface heat flux on the convective boundary layer. Pino et al. (2006) examined the effect of wind shear, inversion strength, and boundary-layer depth on the decay of convective turbulence for cases in which the surface heat flux was also instantaneously removed. Goulart et al. (2003) developed a dynamical energy spectrum model to study the decay of convective turbulence. The model results were validated with LES data. More recently, Goulart et al. (2010) used an improved version of their dynamical model to investigate the influence of near-surface shear production on the decay of turbulent kinetic energy (TKE) at different heights in the ABL. At another scale, a few LES studies have examined the entire diurnal cycle of the ABL. For instance, Brown et al. (2002) studied the development of shallow cumulus clouds over land between 1130 and 0200 UTC. Kumar et al. (2006) modelled the evolution of the ABL over an entire diurnal cycle using realistic surface boundary conditions from the Horizontal Array Turbulence Study (HATS) experiment. The simulation of Kumar et al. (2006) captured the main features of the convective and stable boundary layers, including the formation of a low-level jet at night. Similarly, Basu et al. (2008) modelled the ABL for a complete day of the 1967 Wangara case study.

Previous studies have also used laboratory experiments to investigate the decay of turbulence. For instance, the experiments of Comte-Bellot and Corrsin (1971) and De Silva and Fernando (1994) were designed to analyze the decay of grid-generated nearly-isotropic turbulence. The authors found that the TKE decay in time was well described by a power law. Cole and Fernando (1998) studied the time evolution of temperature and velocity fluctuations in a convective turbulent boundary layer in response to a cooling surface inside a water tank. They found that both the velocity and temperature fluctuations decayed at similar rates. More recently, Kang et al. (2003) performed an update of the

Comte-Bellot and Corrsin (1971) dataset at a higher Reynolds number and compared it with LES using different subgrid-scale models.

There appears to be a substantial lack of literature associated with field experiments that study the decay period. Two of the largest field campaigns designed to study the ABL convective decay were carried out by Grant (1997) over a shallow river valley in the UK and by Acevedo and Fitzjarrald (2001) using a sensor network around Albany airport, New York. Other studies have focused on the evening transition, but not specifically on the decay of convective turbulence. Brazel et al. (2005) and Pardyjak et al. (2009), for instance, studied the evening transition around Phoenix, Arizona, with a main focus on thermal circulation patterns and topographic effects. A few authors have studied solar eclipses, in which the external time scales were exceptionally short due to a sudden elimination of the incoming solar radiation (e.g. Dolas et al. 2002; Girard-Ardhuin et al. 2003). One of the motivations behind these studies was to compare atmospheric measurements within the theoretical framework of Nieuwstadt and Brost (1986). Solar eclipses are a rare phenomena that are not necessarily representative of the physical processes typically observed in the atmosphere during a decay period over flat terrain.

When the convective ABL decays, according to Sorbjan (1997), there are two time scales involved: the first is the convective eddy turnover time scale (Deardorff 1970) and the second is the time scale associated with the evolution of the buoyancy forcing at the surface. This external forcing time scale typically lasts several hours on a clear day at midlatitudes. However, in several numerical simulations of convective turbulence decay, very short external forcing time scales are specified. For example, Nieuwstadt and Brost (1986) and Pino et al. (2006) both imposed a sharp cut-off in the surface sensible heat flux H in their LES studies. On the other hand, Sorbjan (1997) used a cosine decrease of H with approximately 1.4 h between the maximum surface heat flux and the time the heat flux reaches zero. In his study, the surface heat flux forcing stopped very shortly after H became negative. Perhaps only Beare et al. (2006) studied the full realistic afternoon and early evening transition periods of the ABL with LES runs between 1200 and 0000 UTC. Their simulation results could reproduce measurements taken over a grass field fairly well.

To date, most of the contributions on the study of the decay of convective turbulence have focused on very short forcing time scales. There is thus a clear need to better understand the turbulence decay over realistic time scales that are observed in the atmosphere. To do so, it is useful to identify the two important transition sub-periods that appear to characterize the complete transitory period. First, the afternoon transition, which is the period when the surface sensible heat flux starts to decrease in response to the reduction in solar radiation. The second sub-period is the early evening transition, which typically begins before sunset, when the sensible heat flux becomes negative. The negative surface heat flux then leads to the development of a stable boundary layer that often grows throughout the night.

Another important consideration in addition to the decay time scales is the influence of surface properties. The diurnal cycle of H is highly dependent on the land-surface characteristics (see Beyrich et al. 2006; Kumar et al. 2010). The different thermal capacities of a heterogeneous landscape will result in spatially-varying cooling rates during the decay period. For example, an urban area will cool down less rapidly than a grass field. These differences in the time evolution of the surface heat flux will in turn affect the local decay time scales of the TKE k, which is a measure of the intensity of turbulence (Stull 1988).

The primary aim of our study is to better understand the physics of the decay period from both a phenomenological and quantitative perspective; in particular, we investigate turbulent decay over realistic heterogeneous terrain where there is currently a lack of knowledge and field measurements. Herein, we address the effects of terrain on the forcing of turbulence

through the development of a simple surface sensible heat flux model for the afternoon and early evening transition periods that includes negative fluxes. We propose a new function that better represents the behaviour of the sensible heat flux during the entire decay period and validate it with eddy-covariance measurements over different land-surface types. We compare a traditional cosine decay of H with a complementary error function fit. In the second part of the paper, we test a simple model for the decay of TKE that uses only two terms on the right-hand side of the k-budget equation: dissipation and buoyancy production or consumption. The buoyancy term is then modelled using the new function for $H(t)$. This model for the surface sensible heat flux is fairly general and could be used to force more complicated models (e.g. LES) where it may not be feasible to solve the entire surface energy budget.

2 Background

The TKE k within the convective boundary layer is an extremely important quantity and serves well for tracking the decay of atmospheric turbulence. Its time average is defined as $\bar{k} = \frac{1}{2} \left(\overline{u'^2} + \overline{v'^2} + \overline{w'^2} \right)$. The TKE budget equation in the atmosphere may be written, using index notation, as (following Stull 1988):

$$\frac{\partial \bar{k}}{\partial t} + \overline{u_j} \frac{\partial \bar{k}}{\partial x_j} = \delta_{i3} \frac{g}{\theta_v} (\overline{u_i' \theta_v'}) - \overline{u_i' u_j'} \frac{\partial \overline{u_i}}{\partial x_j} - \frac{\partial (\overline{u_j' k})}{\partial x_j} - \frac{1}{\rho} \frac{\partial (\overline{u_i' p'})}{\partial x_i} - \varepsilon, \qquad (1)$$

where t is time, i and j are indices to sum over, u is the wind speed, g is the gravitational acceleration, θ_v is the virtual potential temperature of air, ρ is the air density, p is pressure and ε is the dissipation rate of the TKE.

Following Nieuwstadt and Brost (1986), (1) can be simplified during the period when the convective boundary layer is decaying if the following assumptions are made: there is no vertical gradient of k, there is very little shear production of turbulence, subsidence and the pressure fluctuations can be neglected and the flow is horizontally homogeneous. Assuming an abrupt shut-off of the buoyancy flux prior to the decay period, then the equation for the TKE averaged across the boundary layer $\langle \bar{k} \rangle$ may be simplified from (1) to:

$$\frac{\partial \langle \bar{k} \rangle}{\partial t} = -\langle \varepsilon \rangle. \qquad (2)$$

The above equation is valid from $t = t_0$ (where t_0 is the start of the decay) until the end of the decay period; the dissipation term ε is always a sink of k. Nieuwstadt and Brost (1986) parameterized ε as follows:

$$\langle \varepsilon \rangle = C_\varepsilon \frac{\langle \bar{k} \rangle^{3/2}}{h}, \qquad (3)$$

where the constant $C_\varepsilon \approx 2$ and h is the boundary-layer depth. The above equation is subject to the following initial conditions: $\langle \bar{k} \rangle (t = t_0) = C^2 w_*^2$ where it was assumed that the dissipation length scale during the decay process remains proportional to the initial value of h and $C \approx 0.55$. Nieuwstadt and Brost (1986) showed that, for an abrupt shut-off of the buoyant production, the decay of TKE appears to scale with the boundary-layer depth and the Deardorff convective velocity w_* both observed at the beginning of the decay period.

The scaling parameter w_* is defined as:

$$w_* = \left(\frac{g h_0}{\overline{\theta_{v0}}} \overline{w'\theta_{v0}'} \right)^{1/3},$$ (4)

where all the variables with the subscript 0 are evaluated at $t = t_0$. Using the convective scaling, the eddy turnover time scale is given by:

$$t_* = \frac{h}{w_*}.$$ (5)

Thus, solving (3) between $t = t_0$ and the end of the decay period, the following result is obtained:

$$\frac{\langle \overline{k} \rangle}{w_*^2} = \left(\frac{C_\varepsilon}{2} \frac{t' w_*}{h} + \frac{1}{C} \right)^{-2},$$ (6)

where $t' = t - t_0$. Equations (2), (3) and (6) are valid for averages taken over the entire boundary-layer depth. For a boundary layer dominated by convection, if we assume that the volume-averaged k is subject to a progressive decrease of the buoyant production during the decay period, we have the following equation for $\langle \overline{k} \rangle$:

$$\frac{\partial \langle \overline{k} \rangle}{\partial t} = \frac{1}{h} \int_0^h \frac{g}{\overline{\theta_v}} (\overline{w'\theta_v'}) \, dz - \langle \varepsilon \rangle.$$ (7)

Assuming a linear decrease in the buoyancy flux (e.g. Stull 1988) from the surface value $\overline{w'\theta_v'}|_s$ to $-A\overline{w'\theta_v'}|_h$ at h (which should be strictly valid only at the beginning of the decay period) yields

$$\frac{\partial \langle \overline{k} \rangle}{\partial t} = \frac{1}{2} (1 - A) \frac{g}{\overline{\theta_v}} (\overline{w'\theta_v'}) \bigg|_s - C_\varepsilon \frac{\langle \overline{k} \rangle^{3/2}}{h},$$ (8)

where A is a constant typically ranging between 0.1 and 0.3 (Stull 1988). The buoyancy term can have either a positive or negative sign. During most of the daylight hours, it is positive and contributes to the production of k. During the evening and night, it is usually negative and thus contributes to the loss of k. For a relatively dry boundary layer, it is reasonable to assume that $\overline{w'\theta_v'} \approx \overline{w'\theta'}$ (for a wet ABL, the difference between the two can be up to 10%). This assumption allows one to use the sensible heat flux, defined as $H = \rho c_p \overline{w'\theta'}|_s$ where c_p is the specific heat of air, which can then be framed in the context of the surface energy balance (see Sect. 3.2). While (8) has a theoretical basis, it is difficult to validate given the paucity of data in the boundary layer during the decay of the convective boundary layer. Hence, we propose the following alternative heuristic model for the decay of k at a point in the surface layer, which can be validated with surface-layer measurements:

$$\frac{\partial \overline{k}}{\partial t} = \frac{g}{\overline{\theta_v}} (\overline{w'\theta_v'}) - \varepsilon.$$ (9)

Again, we assume a dry boundary layer (i.e., $\overline{w'\theta_v'} \approx \overline{w'\theta'}$ and $\overline{\theta_v} \approx \overline{\theta}$). In (9), the buoyancy flux and ε must be modelled. The buoyancy flux is modelled as described in Sect. 3.2, however the dissipation rate has proven more challenging. In the surface layer, one expects ε to follow surface-layer scaling using u_* and z. However, extensive testing (see Sect. 4) has revealed that over a range of surface types, boundary-layer depths and fluxes, the parametrization of ε using (3) with the same constants and surface-layer measurements of k performs

Table 1 List of micrometeorological stations from the LITFASS-2003 field campaign used in this study

Station	Latitude (°N)	Longitude (°E)	Elevation above mean sea level (m)	Measurement height above ground (m)
Barley	52.192	14.116	86	3.25
Maize	52.174	14.122	75	3.25
Triticale	52.137	14.177	52	3.55
Forest	52.182	13.953	49	30.6
Rapeseed 1	52.154	14.103	67	3.40
Rapeseed 2	52.124	14.174	48	3.50
Grass 1	52.166	14.122	73	2.40
Grass 2	52.166	14.122	73	2.40

extraordinarily well. Note that, for many realistic decay situations, shear production exists and is expected to play a dominant role in the TKE equation near the surface (e.g. Goulart et al. 2010). Hence, the model presented here for TKE decay is expected to be valid only for conditions of strong convection and weak synoptic forcing.

In Sect. 4.1, we test two different equations to model H during the decay period and validate them with measurements over different surface types. Then in Sect. 4.2 we evaluate $k(t')$ based on the numerical integration of (9) and compare it against field measurements.

3 Methods

3.1 Eddy-Covariance Measurements

To study the afternoon and early evening variations of the sensible heat flux over different surface types, we used measurements collected during the LITFASS-2003 experiment (Lindenberg Inhomogeneous Terrain-Fluxes between Atmosphere and Surface: a long term study). This intensive field campaign was conducted over a 30-day period from May to June 2003 in eastern Germany. The 20×20 km^2 study area consisted of various land surfaces including forests, crop fields, lakes, grass and urban areas. A total of 13 micrometeorological stations were deployed over this heterogeneous landscape to measure the turbulent fluxes of heat and momentum. More details about the experiment are found in Beyrich and Mengelkamp (2006).

Out of the 13 micrometeorological stations deployed, eight were used in our analysis. Four stations were not considered due to insufficient data availability or to the presence of discontinuities in the measurements. Data from the only station located over a water body were also excluded. Indeed, the diurnal cycle of sensible heat flux over water contrasts with what is typically observed over land due to a different partitioning of the energy at the surface. Consequently, the decay of convective turbulence over water bodies is likely to differ from that observed over land surfaces, and thus is beyond the scope of our paper. The eight stations selected were distributed over several surface types (mostly crops): barley, maize, triticale, forest, rapeseed and grass (see Table 1). Note that the stations grass 1 and 2 are located next to each other. An excellent discussion on the variability of the surface fluxes can be found in Beyrich et al. (2006). All eddy-correlation measurements were made in the inertial sublayer.

Because the stations were close to each other, they were approximately exposed to the same incoming shortwave radiation S_d. Based on S_d and cloud-cover data obtained at one location inside the LITFASS-2003 study area, three clear-sky days were identified: 29 May, 30 May and 1 June 2003. These 3 days were associated with anticyclonic conditions and light easterly winds. Due to the relatively high latitude of the site ($\approx 52°$N) and the proximity in time with the summer solstice, the selected days had a significant number of daylight hours. As an indication, the official local sunrise and sunset for 30 May 2003 were 0451 and 2112 local summer time, respectively. The sensible heat-flux measurements were averaged over the 3 days to obtain one diurnal cycle of H for each station.

The effect of soil moisture on the partitioning of the energy at the surface was not explicitly determined in our analysis. It is known that wet soil affects the albedo of the surface and thus its absorption of the incoming solar radiation. A wetter soil leads to enhanced evaporation and thus to a greater latent heat flux $L_e E$ in the atmosphere, where L_e is the latent heat of vaporization of water and E is the evaporation. Over the three selected clear-sky days, the average midday Bowen ratio (Bo $= H/L_e E$) was a maximum over forest (Bo $= 8$) and a minimum over rapeseed 2 (Bo $= 0.75$). All the other sites had a midday Bowen ratio between 1 and 3 on average.

All meteorological data used in this study were averaged over 30-min segments, and details of the data processing are presented in Beyrich et al. (2006). Note that local summer time is used throughout.

3.2 Modelling the Diurnal Cycle of the Sensible Heat Flux

One of our main objectives is to model the sensible heat-flux variations during the decay period. The first step to achieve this is to properly define this time interval. Then, we present two fitting functions that we compare against the field measurements introduced in Sect. 3.1.

The determination of the decay period is based on the close relationship that exists between the incoming shortwave radiation and the daily variations of sensible heat fluxes. A 'solar' time scale $\tau_{f,\text{solar}}$ is thus defined as the time interval between the maximum solar radiation observed in the day and the extrapolation to zero of a cosine fit of the solar radiation signal (see Fig. 1a). Then, using the sensible heat flux diurnal cycle (see Fig. 1b), a cosine fit of the observations around midday is performed to identify the maximum value. This point, which corresponds to the start of the afternoon transition, marks the beginning of the decay period. The end of the decay period is simply found at a time $\tau_{f,\text{solar}}$ later, typically 1 or 2 h after the beginning of the early evening transition.

To model the diurnal variations of H, two different fitting functions have been tested. The first one is:

$$H_{\text{erfc}}(t') = \frac{(H_{\max} - H_{\min})}{2} \left[\text{erfc} \left(\frac{t'}{\tau_{\text{erfc}}\sqrt{2}} - \frac{3}{\sqrt{2}} \right) \right] + H_{\min}, \qquad (10)$$

where $H_{\text{erfc}}(t')$ is the sensible heat flux predicted by the erfc function, $H_{\max}$ is the maximum sensible heat flux observed at midday, $H_{\min}$ is the minimum sensible heat flux observed during the decay period, which might be slightly different from the minimum H over the entire day (e.g. Fig. 1b), t' is the time in hours after the start of the decay process and τ_{erfc} is a decay time scale. Note that the complementary error function erfc is defined as $\text{erfc}(x) = 1 - \text{erf}(x)$, where $\text{erf}(x)$ is the error function (see Abramowitz and Stegun 1965).

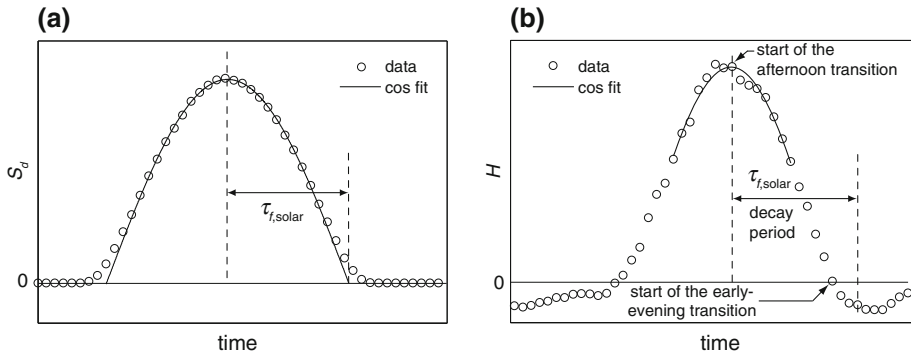**Fig. 1** **a** Sample diurnal cycle of the global incoming shortwave radiation S_d. *Circles* show data points for this arbitrary case. The *solid line* is a cosine fit of the observations. The extrapolation of this fit to zero is used to determine the solar time scale $\tau_{f,\text{solar}}$. **b** Sample diurnal cycle of the sensible heat flux H. *Circles* show data points for this arbitrary case. The *solid line* is a cosine fit of the observations. The maximum of this fit is used to set the starting point of the decay period. The end of the decay period is observed at a time $\tau_{f,\text{solar}}$ later

The second fitting function, which has been traditionally used (Sorbjan 1997; Pardyjak 2001; Goulart et al. 2003), is:

$$H_{\cos}(t') = H_{\max}\cos\left(\frac{\pi t'}{2\tau_{\cos}}\right), \tag{11}$$

where $H_{\cos}(t')$ is the sensible heat flux predicted by the cosine function, $H_{\max}$ is the maximum sensible heat flux observed at midday and $\tau_{\cos}$ is a decay time scale. It is important to note that in (11) there is one less fitting parameter than in (10). In all cases, the fitting parameters were found by means of a non-linear least squares analysis with bounded intervals using the Matlab® curve-fitting toolbox.

4 Results and Discussion

4.1 Modelling the Decay of the Surface Sensible Heat Flux

The diurnal cycles of sensible heat flux and solar radiation observed at the eight stations of interest are presented in Fig. 2. As discussed earlier, the site received more than 16 h of sunlight during the selected days as can be seen from the incoming shortwave radiation signal. The solar time scale for the period shown is $\tau_{f,\text{solar}} = 7.35$ h.

Due to the details of the local energy balance, we expect $H_{\max}$, $H_{\min}$ and $\partial H/\partial t$ to vary from site-to-site, and this is discussed at length in Beyrich et al. (2006). Over land and for clear-sky conditions, it is expected that the turbulent heat fluxes follow the diurnal evolution of the solar radiative energy supply. Stable conditions prevailed before sunrise, with negative heat fluxes of approximately -10 to -30 W m^{-2} for all sites. Just after 0600, thus more than 1 h after sunrise, the surface sensible heat fluxes became positive. The time derivative of H was then variable from one site to another. It was very large over the forest, where H went from -15 to 415 W m^{-2} in less than 7 h. At other sites the increase of H was more progressive and the maximum value reached was considerably smaller. For instance, over grass the magnitude of the sensible heat flux was 150 W m^{-2}, whereas over barley or
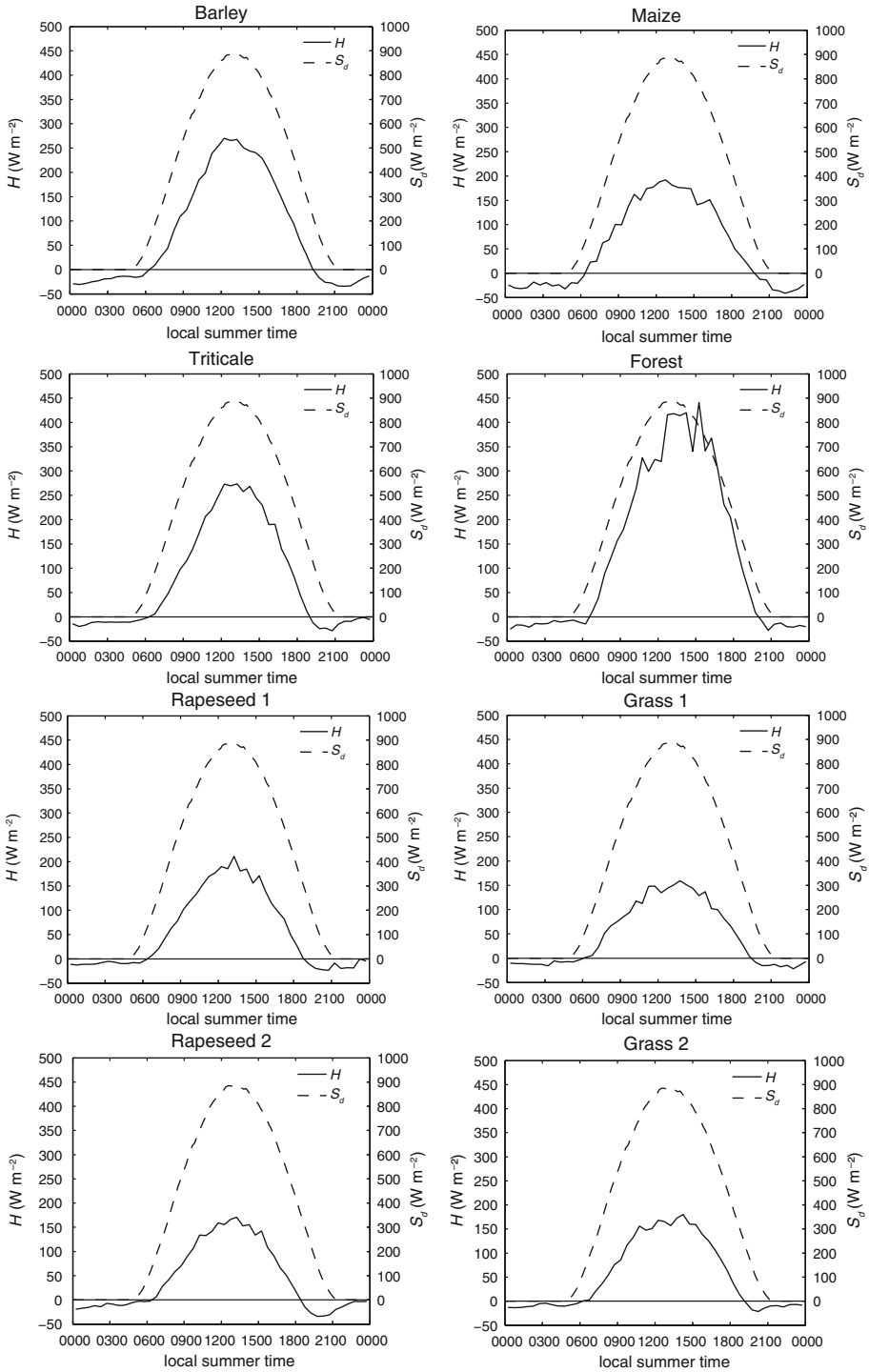
Fig. 2 Diurnal values of the sensible heat flux H (*solid curve*, left axis) and the downward component of shortwave radiation S_d (*dashed curve*, right axis) over several surface types
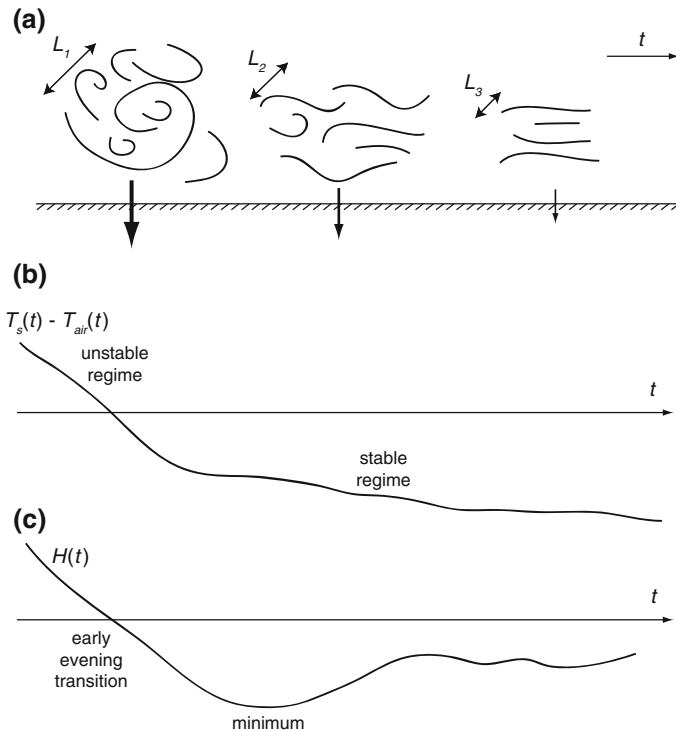
Fig. 3 Schematic representation of the land-atmosphere heat-transfer dynamics around the early evening transition, with: **a** atmospheric turbulence and efficiency of heat transfer with the surface; **b** time evolution of the land-atmosphere temperature gradient; **c** time evolution of the sensible heat flux

triticale it was approximately 250 W m^{-2}. In the second part of the day, the sensible heat flux began to decrease in response to the diminishing incoming solar radiation. The afternoon transition started between 1245 and 1345 (see also Fig. 4), and over the forest it began 1 h later than over rapeseed. The evening transition, following the change in sign of H, began approximately 2 h before sunset. At this time, the sensible heat flux becomes negative and as a result, a stable boundary layer begins to form.

A maximum in downward heat flux was typically observed approximately one and a half hours after the start of the early evening transition. This was particularly obvious over triticale, rapeseed 2 and barley. This well-known feature of the transitional sensible heat-flux cycle (e.g. Caughey et al. 1979) is summarized in Fig. 3. Just after H becomes negative, the sensible heat flux decreases rapidly (as a result of efficient heat transfer to the surface, see Strang and Fernando (2001) and Pardyjak et al. (2002)), and the atmosphere becomes stably stratified. The light winds that are typically observed in the early evening limit the mechanical mixing of the atmosphere and promote the development of a stable boundary layer, with the magnitude of the downward H reduced and eventually fluctuating around values closer to zero for the rest of the night. As a result of this series of events, there is often a minimum in the surface sensible heat flux 1–2 h after the start of the early evening transition. In the next section we present a function that captures this decrease in H.

Figure 4 shows the two fitting functions tested to match the decrease of the sensible heat observed between midday and early evening. The erfc function tends to be a little too flat in
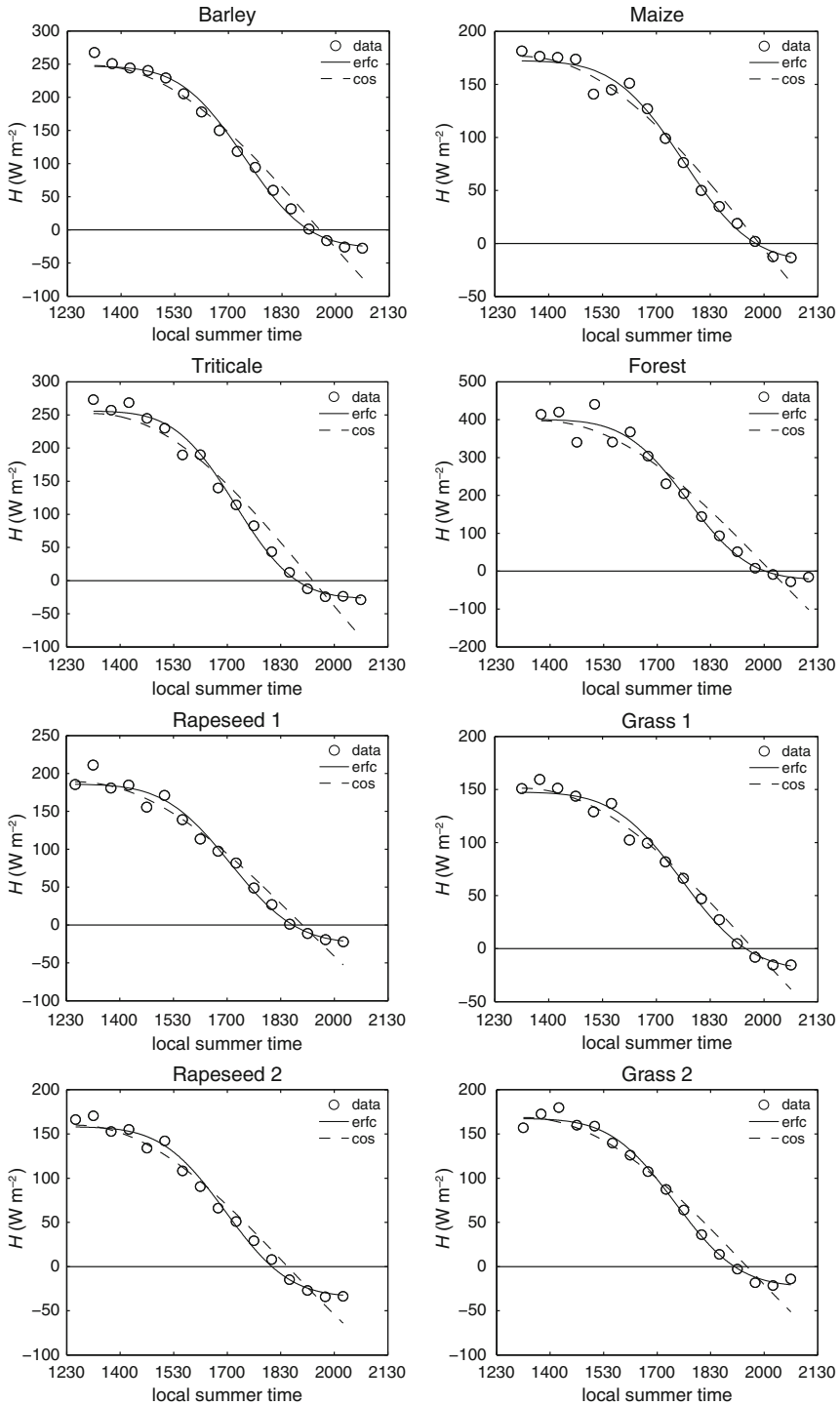
Fig. 4 Comparison of the two different curve fitting functions to capture the midday to early evening decrease of sensible heat flux. Note that the sensible heat flux range is different from one plot to the other

Table 2 Sensible heat-flux modelling parameters at each station for the erfc and cosine models, where H_{max} is the maximum sensible heat flux fitted at midday, H_{min} is the minimum sensible heat flux fitted during the decay period, τ_{erfc} and τ_{cos} are the decay time scales associated with the erfc and cosine models, respectively

Station	erfc			cos	
	H_{max} (W m^{-2})	H_{min} (W m^{-2})	τ_{erfc} (h)	H_{max} (W m^{-2})	τ_{cos} (h)
Barley	246.9	−26.8	1.40	247.9	6.31
Maize	172.5	−17.0	1.50	176.4	6.62
Triticale	256.1	−27.2	1.33	252.1	6.15
Forest	400.7	−23.0	1.37	396.9	6.44
Rapeseed 1	186.0	−24.3	1.45	189.1	6.36
Rapeseed 2	158.2	−34.2	1.40	160.0	5.94
Grass 1	147.6	−19.9	1.49	151.3	6.45
Grass 2	167.6	−22.7	1.42	168.6	6.27

Note that these two time scales are not equivalent by definition, as can be seen by inspecting (10) and (11). As a result, they cannot be compared with each other. For all cases, $\tau_{f,solar} = 7.35$ h

the first portion of the curve and underestimates the maximum sensible heat flux. However, it captures the positive curvature at the transition between the unstable and stable regimes very well. The trough in the sensible heat flux is poorly captured by the cosine fit, which tends to greatly overestimate the magnitude of the minimum sensible heat flux. For instance, over forest there is a difference of 500% between the cosine fit and the measurements around the last data point. The cosine function also underestimates the maximum sensible heat flux, but its time derivative better matches the observations a few hours after the start of the afternoon transition. The occurrence of the change in sign of H is better predicted by (10) than by (11), especially over triticale. The different curve fitting parameters obtained are presented in Table 2.

The H_{max} obtained with the cosine fit, although very close to that obtained with the erfc function, tends to be slightly greater. In terms of the decay time scales observed, typically $\tau_{erfc} \approx \tau_{f,solar}/5$ and $\tau_{cos} \approx 4\tau_{f,solar}/5$. It is also interesting to compare the variability of the different parameters among the surface types. For instance, the magnitude of the H_{min} over rapeseed 2 is twice that observed over maize. Because the different surface types have different thermal properties, the decay time scales also vary from site to site, as can be seen in Fig. 4.

To quantitatively evaluate the performance of each fitting function, we used the normalized root-mean-square error (NRMSE), defined as:

$$NRMSE = \frac{\sqrt{\sum_{i=1}^{n} \frac{(H_{fit,i} - H_{data,i})^2}{n}}}{H_{max} - H_{min}}. \tag{12}$$

The distribution of NRMSE is presented in Fig. 5. For all stations the *NRMSE* is smaller than 10%, which means that both functions capture the decrease of surface heat flux in the second part of the day relatively well. However, the erfc fit is clearly more precise as its NRMSE is smaller than the cosine fit in all cases. Significant differences between the two fitting functions can be observed over triticale and grass 1, where the NRMSE is reduced by a factor of 2. The erfc fit yields a mean *NRMSE* of 3.86% whereas the cosine fit has a mean value of *NRMSE* of 6.34%. Based on this, we conclude that the erfc model (see (10)) is more suitable than the cosine model (see (11)) for capturing the time evolution of sensible heat
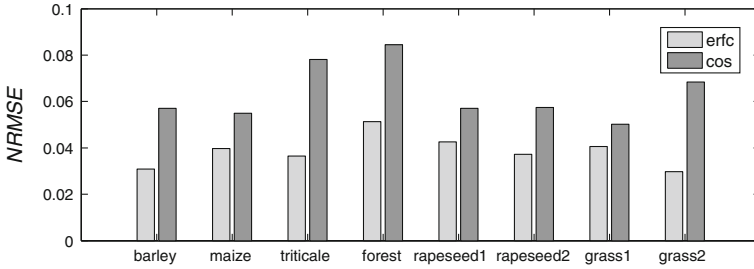
Fig. 5 Distribution of the normalized root-mean-square error for the two fitting functions
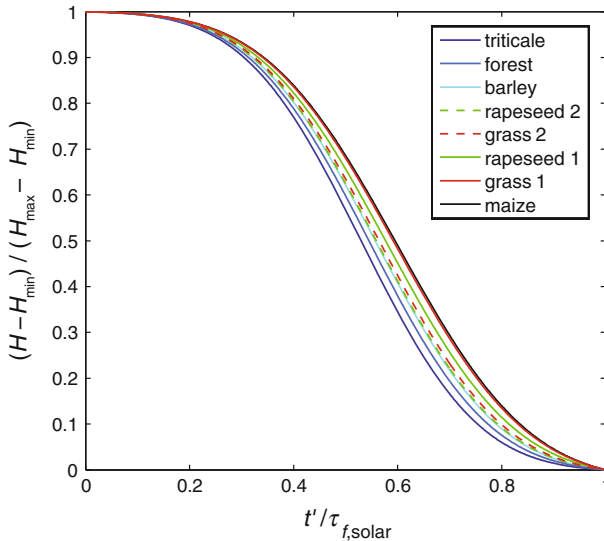

Fig. 6 Normalized sensible heat-flux evolution illustrating the different decay time scales of H at each station using the erfc function (see (10))

flux in the afternoon and early evening periods. The cosine function (see (11)) could also be used in some cases, but only when the sensible heat flux has not yet changed sign.

Figure 6 shows the different normalized values of the fitted surface heat-flux evolution using the erfc function (see (10)) during the decay period. The ordinate shows the difference between the evolving surface heat flux $H(t')$ and its minimum value normalized by the range of surface heat fluxes observed. On the abscissa the time is normalized by the solar forcing $\tau_{f,\text{solar}}$. With two of the three fitting parameters used in the normalization, this figure emphasizes the variations of τ_{erfc} over the different surface types. Around $t'/\tau_{f,\text{solar}} = 0.5$, the normalized values of H observed vary by about 10%. We observed that the forest and triticale surfaces cooled down the most rapidly, and maize and grass cooled the least rapidly. This behaviour of the maize and grass surfaces may be attributed to a stronger coupling with the soil. Both these types of vegetation were fairly low in height (with large sections of bare soil between the maize plants) during the measurement period, resulting in a greater heat supply from the soil during the transition periods. All other plants were taller, thus they may not have benefited from this heat supply.

4.2 Comparison of the Turbulent Kinetic Energy Model with Surface-Layer Observations

In the previous section, we presented two functions selected to capture the diurnal variations of the sensible heat flux. This simple model for $H(t')$ could be used in many applications. In this study, we wish to estimate the TKE during the decay period. The objective of the current section is thus to test the TKE model (see (9)) developed in Sect. 2 using (10) and (11) for $H(t')$ against field measurements.

To demonstrate that our method is robust, we validated it against field observations collected over a wide range of surface types and conditions. The modelled TKE was first compared to experimental data from the LITFASS-2003 campaign taken on 1 June 2003 over four surface types: barley, forest, grass and rapeseed. The TKE model was also tested with eddy-covariance data taken in the surface layer over a desert (Great Salt Lake Desert, Utah) and over a residential area (Murray, Utah). These two landscapes are very different from one another and from the land-surface types present in the LITFASS-2003 domain. Over the desert, the aerodynamic roughness length is small ($z_0 \approx 1$ mm) and the surface is homogeneous. Consequently, the production of kinetic energy is likely to be dominated by buoyancy fluctuations (free convection regime) during the daytime. The Bowen ratio is very large as evaporation is low. Over the residential area, the aerodynamic roughness length is much larger ($z_0 \approx 1$ m) and the surface is very heterogeneous, so the contribution of wind shear to the TKE generation is not likely to be negligible. This allowed us to test (9) for cases closer to the forced convection regime. Over the residential area, the Bowen ratio is close to unity due to the presence of vegetation (in parks and courtyards).

To model $k(t')$ using our approach, the following ABL variables are needed: the near-surface air potential temperature $\overline{\theta}$, the boundary-layer height h and, if possible, the incoming solar radiative flux S_d to determine the forcing time scale. Both $\overline{\theta}$ and h have to be determined around the afternoon transition. In our case, $\overline{\theta}$ was measured by sonic anemometers located in the inertial sublayer. Obtaining the boundary-layer depth h was a more challenging task. At the LITFASS site, radiosondes were regularly launched in the vicinity of the two stations over grass (52.166°N, 14.122°E). In the desert and suburban sites, the nearest atmospheric soundings were performed at the Salt Lake City airport ($\approx$125 km to the north-east of the desert site; $\approx$15 km north of the suburban site). One of the two daily soundings is taken at 1800 LST, which is typically a few hours after the beginning of the afternoon transition. Variations in the boundary-layer height in these few hours had to be neglected. Only profiles in which the surface layer, the mixed layer and the entrainment layer could be clearly identified were retained.

To determine the forcing time scale $\tau_{f,\text{solar}}$, we used the method described in Sect. 4.1. Unfortunately, no incoming shortwave radiation data were available at the desert and suburban sites. However, in the LITFASS-2003 study, in which incoming shortwave data were available, we noted that the measurements closely matched theoretical values calculated based on Stull (2000). This theoretical method was thus used to calculate the incoming shortwave radiation at the desert and suburban sites. This is a very robust and convenient method to determine the forcing time scale $\tau_{f,\text{solar}}$ of the decay period, since the only inputs required are the coordinates of the site and the date.

To test the TKE model, days with clear-sky conditions and weak synoptic activity were selected. For the LITFASS-2003 dataset, we selected one of the three days used for the analysis in Sect. 4.1. At the two other sites, as no incoming shortwave radiation data were directly available, we selected days without discontinuities in the net radiation diurnal cycles, an indication of cloud-free conditions. In the end, two days were selected at the desert and suburban sites.

Table 3 Important initial (at $t' = 0$) ABL parameters and time scales on 1 June 2003 over four surface types from the LITFASS-2003 dataset

For all cases, $h = 1072$ m and $\tau_{f,\text{solar}} = 7.35$ h

Station	Initial ABL quantities		
	w_* (m s^{-1})	t_* (min)	u_* (m s^{-1})
Barley	1.94	9.21	0.22
Forest	2.34	7.63	0.48
Grass 1	1.69	10.54	0.21
Rapeseed 1	1.93	9.24	0.40

4.2.1 TKE Decay Over a Forest, Grass and Crop Fields

The TKE measured on 1 June 2003 over forest, barley, grass (station 1) and rapeseed (station 1) during the LITFASS-2003 experiment was used to validate the TKE model. Note that the details of the curve fits for the sensible heat flux are not presented here as the results are very similar to what is found in Sect. 4.1 (where we used an average of $H(t)$ over 3 days).

Some of the important ABL scaling variables at the start of the decay period are reported in Table 3. As expected, the friction velocity u_* is greatest over the forest, whereas over barley and grass it is approximately twice as small. The convective velocities are all in the expected range of values for a midlatitude site under sunny conditions (Stull 1988).

The decay of TKE is plotted in Fig. 7, noting that there are no values before $t'/t_* \approx 2$ because 30-min averages of k are used. A few observations are important to point out. First, the time scale of the decay is much larger than that predicted by (6) for the averaged k over the entire boundary layer. The importance of realistic time scales for the decay of sensible heat flux has been discussed already in Sect. 4.1. As the buoyancy production $g\overline{(w'\theta')}/\overline{\theta}$ is a critical component of the TKE budget, the time scales associated with H are closely related to the decay time scales of k.

In the two models of $k(t')$, there is an increase in k between $t'/t_* = 0$ and $t'/t_* = 1$, when the sensible heat flux is not significantly different from its initial value. Consistent with previous work (e.g. Sorbjan 1997), the models reveal that it takes about one eddy turnover time for the TKE to reach a constant value before the decay starts. Surprisingly, there is very little difference between using a cosine function or an erfc function to model $k(t')$. We hypothesize that this lack of model sensitivity to the exact shape of $H(t')$ indicates that the most important parameters in modelling $H(t')$ are the magnitude of the decrease in $H(t')$ and the forcing time scale.

Around the early evening transition, the decay rate is much faster than predicted by (6). Even though there is not yet a theoretical basis for this rate of TKE decay, however, we have added a solid line with a decay rate as t^{-6} in Fig. 7 to emphasize the sudden collapse of turbulence during this period.

Over each of the four surface types, the modelled TKE using (9) matches reasonably well the surface-layer measurements. The agreement between the model and the data is excellent over the grass and forest sites; over barley and rapeseed 1, however, the midday TKE is underestimated, while the model tends to slightly anticipate the sudden decrease in TKE.

4.2.2 TKE Decay Over a Desert

We analyzed the decay of TKE in the surface layer over a desert, using data from the SGS 2002 experiment (see Higgins et al. 2007). These measurements were collected at the Surface
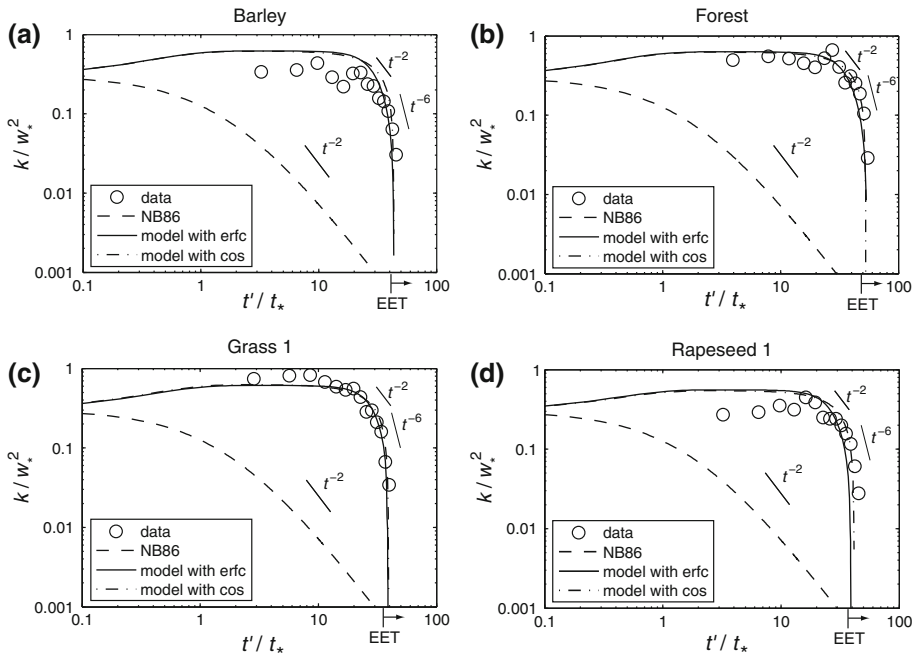
Fig. 7 Decay of turbulent kinetic energy on 1 June 2003 at a few LITFASS-2003 stations: **a** barley, **b** forest, **c** grass 1 and **d** rapeseed 1. The *circles* show experimental data points. The *dash curve* is the Nieuwstadt and Brost (1986) model for $k(t')$ (dissipation term only) applied to the surface layer. The two other curves are outputs from our model for $k(t')$, which includes both the buoyancy fluctuations and the dissipation. The *solid curve* uses (10) and the *dash-dot curve* uses (11) for $H(t')$. Note that the minimum values of our modelled k are undefined at some point after the start of the early evening transition (EET)

Table 4 Important initial (at $t' = 0$) ABL parameters and time scales for the two selected days over the desert

Date	Initial ABL quantities				Time scale
	h (m)	w_* (m s^{-1})	t_* (min)	u_* (m s^{-1})	$\tau_{f,solar}$ (h)
11 July 2002	1571	1.83	14.3	0.22	6.63
21 July 2002	845	1.54	9.2	0.25	6.52

Layer Turbulence and Environmental Science Test (SLTEST) site situated at the southern tip of the salt flats of the Great Salt Lake Desert (40.142°N, 113.458°W). The sonic anemometer used in this study was located 2.3 m above the ground. For more details about the SLTEST site, see Metzger and Holmes (2008). At the SLTEST site, 2 days met the selection criteria for our analysis: 11 July and 21 July 2002. The important initial ABL quantities and time scales for these 2 days are presented in Table 4. Note that the initial boundary-layer height was particularly low on 21 July 2002 ($h = 845$ m), but was still within the range of expected values for this type of environment. The midday friction velocities were relatively small (<0.3 m s^{-1}) on both days, which is typical of atmospheric flow over a smooth surface.

Figure 8 shows the diurnal cycle of the sensible heat flux and the fitting functions for the two selected days. The afternoon transition started around 1430 local time and the decay
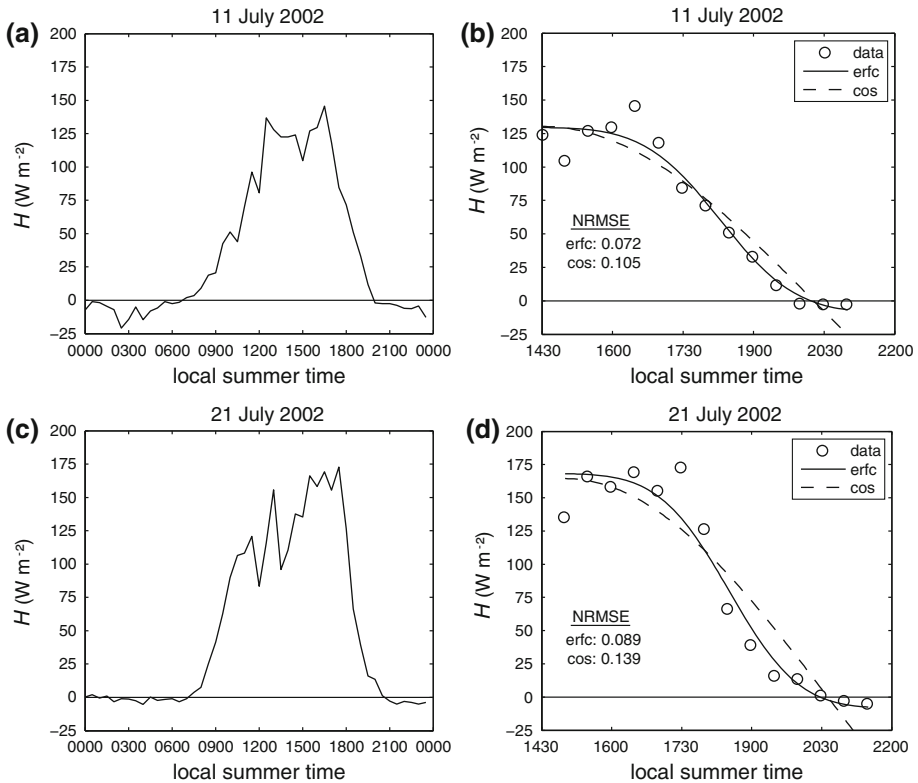
Fig. 8 *Left*: sensible heat flux measurements taken over the desert site on **a** 11 July 2002 and **c** 21 July 2002. *Right*: comparison of the two different curve fitting functions during the decay period on **b** 11 July 2002 and **d** 21 July 2002. The NRMSE is indicated on the plots of the right column

period ended around 2100. On 11 July 2002, neither of the two functions properly captures the start of the early evening transition. On 21 July 2002, however, the timing of the change in sign of $H(t')$ is correctly reproduced by the two fitting functions. As discussed in Sect. 4.1, the erfc function has a much smaller error than the cosine fit when the sensible heat flux is negative. As seen in Fig. 8, the NRMSE is smaller for the erfc fit than for the cosine fit in the two cases. Overall, the NRMSE values are larger than those reported in Sect. 4.1 since the sensible heat-flux data were not smoothed by a multi-day average. However, the NRMSE results appear sufficiently low (<15%) to allow for the use of the sensible heat-flux fits for modelling k.

The decay of TKE over the desert site is presented in Fig. 9, and as mentioned previously, there are no values before $t'/t_* \approx 2$ because 30-min averages of k are used. Note that in both cases the predicted kinetic energy suddenly falls to extremely small values (beyond the axis limits) around the early evening transition (a feature also present in Fig. 7). This is investigated in Fig. 10, where we explore the balance between the buoyant production of k and the turbulent dissipation in (9) for the desert site on 21 July 2002. From this figure, it is clear that up to $t'/t_* \approx 2$, the buoyancy flux overcomes the dissipation. As a result, the TKE increases, as seen in Fig. 9b. Between this point and $t'/t_* \approx 10$, the difference between the two terms is minimal and consequently k is constant. For $t'/t_* > 10$, the variation of TKE
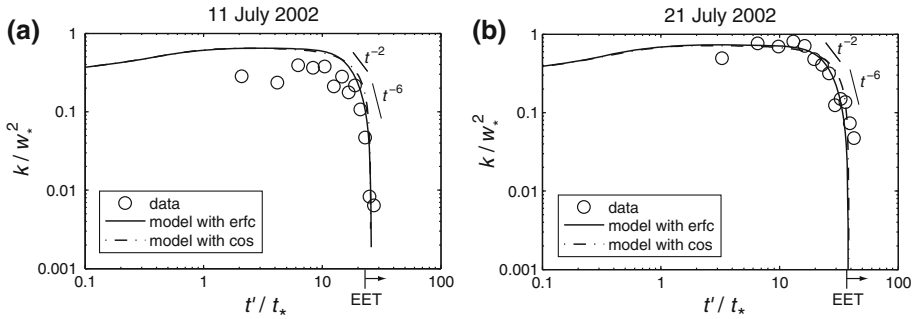
Fig. 9 Decay of turbulent kinetic energy over the desert site on **a** 11 July and **b** 21 July 2002. The measurements were taken at a height of 2.3 m above the surface. The two curves are outputs from our model for $k(t')$, which includes both the buoyancy fluctuations and the dissipation. The *solid curve* uses (10) and the *dash-dot curve* uses (11) for $H(t')$. Note that the minimum values of our modelled k are undefined at some point after the start of the early evening transition (EET)
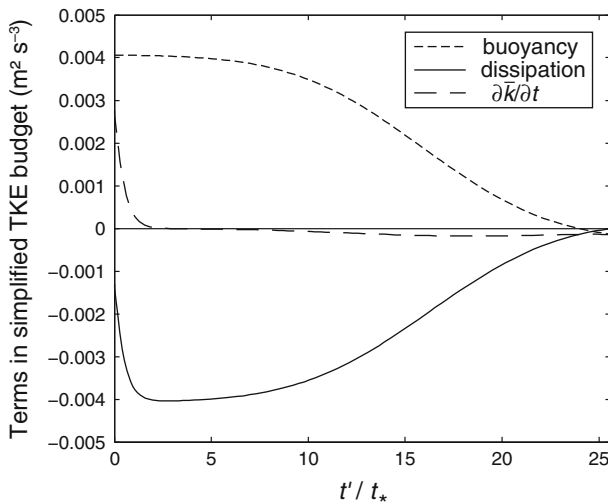

Fig. 10 Comparison between the buoyancy flux and the dissipation in the simplified TKE budget (see (9)) on 21 July 2002 over the desert site. The *short dashed curve* is the buoyant production of k using the erfc model (see (10)), the *solid curve* is the dissipation and the *long dashed curve* is $\partial \overline{k}/\partial t$. Notice that no data are presented for $t'/t_* > 25.6$ since the TKE model is not valid past this point

becomes dominated by dissipation, which leads to the decay of k as previously discussed. When the buoyancy term changes sign, both terms on the right side of (9) act to consume TKE, as k goes to zero. Given that k is by definition a positive quantity, only solutions with k greater than zero are valid.

Another feature of our simple model is its tendency to overestimate the TKE before it decays. This can be due to several factors. First, the height of the boundary layer observed at the Salt Lake City airport could be different than the one at the SLTEST site. For example, a smaller h would tend to lower the modelled TKE and thus better match the data. Ideally, one would want to measure the boundary-layer height around the afternoon transition period. Unfortunately, no sounding data were available at that time. Second, perhaps terms other than
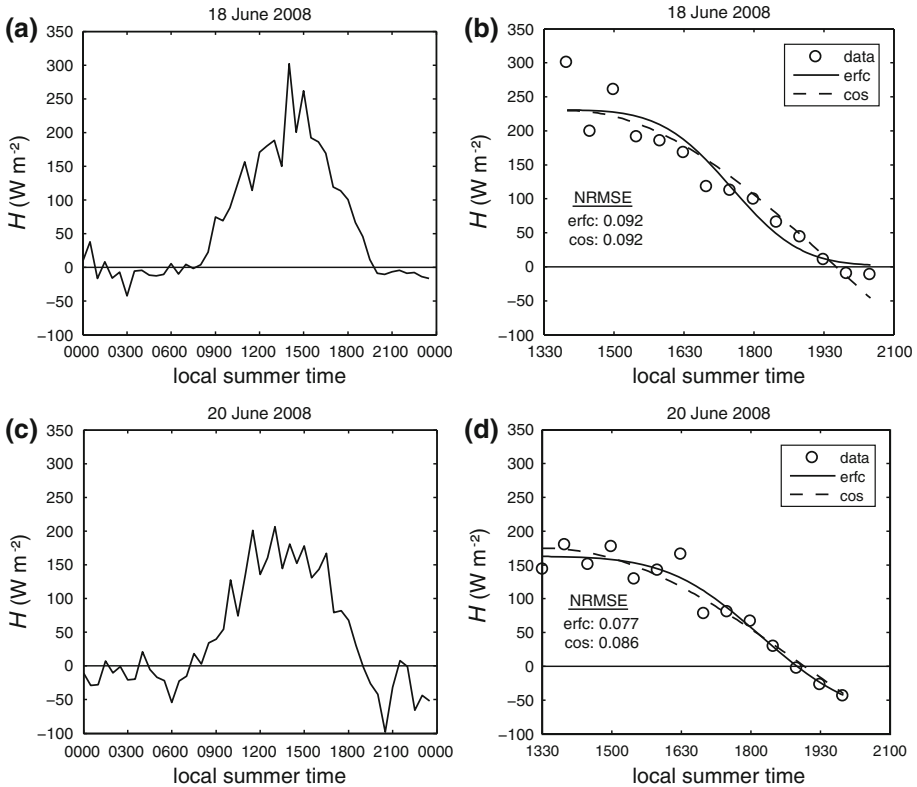
Fig. 11 *Left*: sensible heat flux measurements taken over the suburban site on **a** 18 June 2008 and **c** 20 June 2008. *Right*: comparison of the two different curve fitting functions during the decay period on **b** 18 June 2008 and **d** 20 June 2008. The NRMSE is indicated on the plots of the right column.
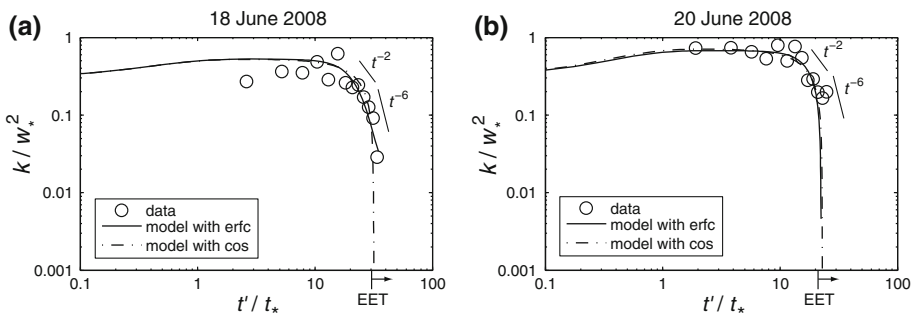

Fig. 12 Decay of turbulent kinetic energy over the suburban site on **a** 18 June and **b** 20 June 2008. The measurements were taken at a height of 35.9 m above the surface. The *circles* show the experimental data points. The two curves are outputs from our model for $k(t')$, which includes both the buoyancy fluctuations and the dissipation. The *solid curve* uses (10) and the *dash-dot curve* uses (11) for $H(t')$. Note that the minimum values of our modelled k are undefined at some point after the start of the early evening transition (EET)

Table 5 Important initial (at $t' = 0$) ABL parameters and time scales for the two selected days over the suburban site

Date	Initial ABL quantities				Time scale
	h (m)	w_* (m s^{-1})	t_* (min)	u_* (m s^{-1})	$\tau_{f,\text{solar}}$ (h)
18 June 2008	1761	2.56	11.5	0.37	6.64
20 June 2008	1923	2.05	15.7	0.71	6.65

dissipation in (1), such as turbulent transport, could be associated with TKE consumption. Nonetheless, in some cases like Fig. 9b, the model captures the time evolution of k fairly well for most of the decay period.

4.2.3 TKE Decay Over a Suburban Area

The suburban eddy-correlation dataset was obtained from a flux station in a residential area in the centre of the Salt Lake valley. The measurements used in this study were collected in the town of Murray, Utah (40.648°N, 111.916°W) located approximately 1300 m above mean sea level. The flux station was installed at 35.9 m above the surface, high enough to reside in the inertial sublayer. The mean building height around the station was approximately 4.4 m. Further information concerning the experimental site can be found in Ramamurthy and Pardyjak (2010). At the Murray site, 2 days met the selection criteria for our study: 18 and 20 June 2008. The important initial ABL parameters and time scales for these 2 days are presented in Table 5. It appears that the ABL scaling variables were within the expected range of values for a typical summertime convective boundary layer in the midlatitudes. The friction velocity was particularly high on 20 June 2008, almost twice as large as that observed on 18 June 2008.

Figure 11 shows the diurnal cycles of surface heat flux for the 2 days studied and the associated curve fits during the decay period. On 18 June 2008, the midday values of H fluctuated significantly, but past 1330 they began a regular decrease. The erfc function does not capture the negative values of H during the early evening transition although the cosine fit does. Nonetheless, the two fitting functions yield the same NRMSE. Around 2030 on 20 June 2008, the sensible heat flux fell abruptly to -100 W m^{-2}, then an hour later returned to values close to zero. This could well be an example of the trough feature of $H(t')$ in the early evening, as discussed in Sect. 4.1. In all cases for the two selected days, the NRMSE values are all smaller than 10%, which suggests that it is appropriate to use these sensible heat-flux fits in the modelling of k.

The TKE evolution for these 2 days is presented in Fig. 12. On 18 June 2008, the model slightly overestimates k but it captures the time at which k starts to decay. The decay rate obtained using the erfc function for $H(t')$ is much closer to the field observations than the model using the cosine function beyond $t'/t_* > 22$. This is caused by the absence of buoyancy consumption in the erfc function, as seen on Fig. 11b. On 20 June 2008, the difference between the model with the erfc fit and the cosine fit is negligible. Except for the three last data points, the simple TKE model matches the observed values of k fairly well.

Even with the previously discussed shortcomings, the proposed TKE model is a significant improvement over using t^{-2}, which was derived for cases in which there is an abrupt shut-off of the surface heat flux. Note that the model captures most of the important part of the decay period very well. It also shows the importance of having a realistic function for
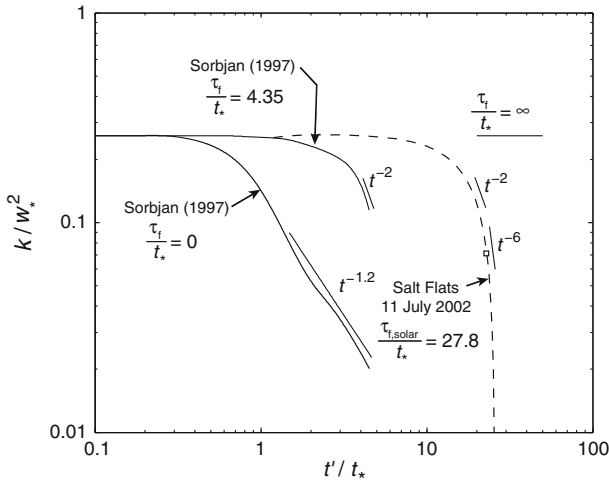
Fig. 13 The two first curves are LES results taken from (Sorbjan 1997). They represent the volume-averaged TKE over the boundary-layer depth. The third curve shows field measurements of TKE taken at a point in the surface layer over the desert site on 11 July 2002. The *square* on the third curve indicates the early evening transition. The TKE values are normalized by the square of the convective velocity when the decay process starts and are a function of t'/t_*. Note that the field measurements are artificially scaled to match the initial value of the two LES runs by Sorbjan (1997)

the diurnal fluctuations of the sensible heat flux in order to properly model the convective atmospheric turbulence decay.

4.2.4 Discussion on Decay Time Scales

As mentioned earlier, the decay time scales of convective turbulence observed in the field differ with what has been traditionally specified in numerical modelling studies (e.g. Sorbjan 1997; Pino et al. 2006), except in Beare et al. (2006). In Fig. 13, we illustrate this discrepancy between modelled decay time scales and measurements.

As discussed in Sorbjan (1997), when $\tau_f/t_* = 0$, the TKE is only a function of t'/t_* and starts to decrease significantly after one eddy turnover time. The other extreme case is when $\tau_f \to \infty$, which implies that the TKE is constant with respect to time. According to Sorbjan (1997), the TKE curves for cases with $\infty > \tau_f/t_* > 0$ should be confined in the space between these two extreme cases. Sorbjan (1997) presents LES results for a case with $\tau_f = 1.4$ h (see second curve from left in Fig. 13). The resulting t_*/τ_f is 4.35.

The external forcing time scale is driven by the solar radiation, as discussed in Sect. 4.1. On a typical summer day at midlatitudes, $\tau_{f,\text{solar}}$ is likely to be approximately 6–8 h. In Fig. 13, field observations over the desert site are presented with $\tau_{f,\text{solar}} = 6.6$ h and thus $\tau_{f,\text{solar}}/t_* = 27.8$. As a result, the TKE starts to decay much later than in Sorbjan's two LES runs, where $t'/t_* \approx 7$ in this particular case. Note how the decay rate goes from t^{-2} to t^{-6}, indicating that the convective decay of turbulence starts slowly. The influence of stable stratification causes a rapid collapse of turbulence at the early evening transition. Note that care should be taken when interpreting Fig. 13, because the LES data from Sorbjan (1997) represent an average over the entire boundary layer and the model for the work presented here is for a single point in the surface layer. LES simulations need to be run to confirm if this behaviour persists after averaging over the entire boundary-layer depth.

5 Conclusions

This study presents a simple model to investigate the decay of the atmospheric TKE during the transition from the daytime to the nighttime regime in the atmospheric surface layer over land. For this model, the decay period is defined by a solar time scale $\tau_{f,\text{solar}}$ based on the incoming shortwave radiative flux. This decay period was found to last several hours at the midlatitude sites of interest during summer. This contrasts with the previous external forcing time scales used in several theoretical studies modelling the decay of the TKE in the ABL. The decay period encompasses: (i) the afternoon transition, when the sensible heat flux starts to decrease after reaching its maximum in the mid-afternoon; (ii) the early evening transition, when the surface heat flux changes sign and turbulent fluctuations are rapidly damped.

Firstly, we described a function well-suited to represent the afternoon and early evening transitions associated with the sensible heat flux. All the fitting parameters (τ_{erfc}, H_{max} and H_{min}) are physically based, and are chosen to capture the buoyancy forcing time scales observed in nature and the influence of surface properties on the magnitude of the heat exchanges. The fitting parameters should ideally be identified through a curve fitting analysis. When no measurements are available, we suggest using $\tau_{\text{erfc}} \approx \tau_{f,\text{solar}}/5$ and determining H_{max} and H_{min} with the help of values found in the literature over similar surface types.

The function for H during the decay period was validated with eddy-covariance measurements taken over different land-surface types during the LITFASS-2003 field campaign. For the period studied, we observed that the forest and the triticale surfaces are the first to cool down, and the maize and grass were the slowest in the cooling process. Midway through the decay period, differences in the relative magnitude of the scaled sensible heat flux could be on the order of 10%, which corresponds to absolute differences of up to 125 W m^{-2} between surfaces such as forest and rapeseed.

Secondly, two models for the decay of TKE k were presented using a simple version of the TKE budget equation in which only the dissipation and the buoyancy fluctuations at the surface were retained. The first was a volume-averaged TKE model, while the second was a heuristic model for a point in the surface layer. Since volume-integrated TKE data were not available, only results from the surface-layer model were presented. However, future experiments should include careful measurements of TKE, dissipation rate and buoyancy flux throughout the boundary layer so that an integral type model can be validated with field data. For the surface-layer model, the dissipation term was defined using the approach of Nieuwstadt and Brost (1986) and for the buoyancy term, fitting functions determined in our study were used. The model was compared against field measurements taken over several surface types: a forest, a grass field, crops, a desert and a suburban area. Generally, the simple model captured the most important features of the TKE decay. The agreement between the simple model for k and the field observations was relatively good (the modelled TKE was always at most within a factor of two of the observed surface-layer values prior to the early evening transition) confirming that the TKE in the surface layer is mostly influenced by the buoyancy fluxes and dissipation in the surface layer under the conditions studied. Following the start of the decay, the modelled TKE was relatively constant for about ten convective eddy turnover times. Then, the TKE displayed a slow decay rate in response to the significant reduction in buoyancy production at the surface, followed by an abrupt decay around the early evening transition. There were no significant differences in the TKE model values when using the erfc or the cosine functions for the time evolution of the sensible heat flux. This shows that in the TKE model, the forcing time scale and the magnitude of the decrease in the buoyancy term are more important features than the specific shape of $H(t')$. The surface-layer model results were presented along with volume-integrated results from

the literature (Nieuwstadt and Brost 1986; Sorbjan 1997) as an instructive comparison. The surface-layer model's performance was particularly surprising given the approach used to approximate the dissipation rate. It appears that the physics embedded in the ratio $\overline{k}^{3/2}/h$ are important for surface-layer scaling under these convectively dominated conditions.

Our analyses of a number of decay datasets with strong convection and weak synoptic forcing indicate that a new theoretical framework might be necessary to describe the TKE budget during the early evening transition, when winds become very light and reduce the role of the mechanical turbulence production. In fact, similar to the data illustrated in Fig. 10, all dynamical budget terms approach zero during the early evening transition, leading to a situation that is very difficult to simulate. This is different to other modelling scenarios (e.g. Pino et al. 2006; Goulart et al. 2010) in which a constant geostrophic forcing ensures that mechanical production is an important term in the surface layer throughout the decay process.

In general cases of atmospheric modelling, including LES over heterogeneous terrain, the complementary error function is suggested (see (10)), because as it reproduces the time evolution of the surface heat flux for the entire decay period fairly well, that is from the afternoon transition to some time after the start of the early evening transition. The cosine function (see (11)) could also be used in some cases, as it includes only two fitting parameters, the maximum heat flux and the forcing time scale, but only for cases in which the atmospheric regime is not yet stable.

References

Abramowitz M, Stegun IA (1965) Handbook of mathematical functions. Dover Publications, New York, 1046 pp

Acevedo OC, Fitzjarrald DR (2001) The early evening surface-layer transition: temporal and spatial variability. J Atmos Sci 58:2650–2667

Basu S, Vinuesa JF, Swift A (2008) Dynamic LES modeling of a diurnal cycle. J Appl Meteorol Climatol 47:1156–1174

Beare RJ, Edwards JM, Lapworth AJ (2006) Simulation of the observed evening transition and nocturnal boundary layers: large-eddy simulation. Q J Roy Meteorol Soc 132:81–99

Beyrich F, Mengelkamp HT (2006) Evaporation over a heterogeneous land surface: EVA_GRIPS and the LITFASS-2003 experiment—an overview. Boundary-Layer Meteorol 121:5–32

Beyrich F, Leps JP, Mauder M, Bange J, Foken T, Huneke S, Lohse H, Ldi A, Meijninger W, Mironov D, Weisensee U, Zittel P (2006) Area-averaged surface fluxes over the LITFASS region based on eddy-covariance measurements. Boundary-Layer Meteorol 121:33–65

Bou-Zeid E, Higgins CW, Huwald H, Meneveau C, Parlange MB (2010) Field study of the dynamics and modelling of subgrid-scale turbulence in a stable atmospheric surface layer over a glacier. J Fluid Mech 665:480–515

Brazel AJ, Fernando HJS, Hunt JCR, Selover N, Hedquist BC, Pardyjak E (2005) Evening transition observations in Phoenix, Arizona. J Appl Meteorol 44:99–112

Brown AR, Cederwall RT, Chlond A, Duynkerke PG, Golaz JC, Khairoutdinov M, Lewellen DC, Lock AP, MacVean MK, Moeng CH, Neggers RAJ, Siebesma AP, Stevens B (2002) Large-eddy simulation of the diurnal cycle of shallow cumulus convection over land. Q J Roy Meteorol Soc 128:1075–1093

Caughey SJ, Wyngaard JC, Kaimal JC (1979) Turbulence in the evolving stable boundary-layer. J Atmos Sci 36:1041–1052

Cheng YG, Parlange MB, Brutsaert W (2005) Pathology of Monin-Obukhov similarity in the stable boundary layer. J Geophys Res Atmos 110:D06101. doi:10.1029/2004jd004923

Cole GS, Fernando HJS (1998) Some aspects of the decay of convective turbulence. Fluid Dyn Res 23:161–176

Comte-Bellot G, Corrsin S (1971) Simple Eulerian time correlation of full- and narrow-band velocity signals in grid-generated 'isotropic' turbulence. J Fluid Mech 48:273–337

De Silva IPD, Fernando HJS (1994) Oscillating grids as a source of nearly isotropic turbulence. Phys Fluids 6:2455–2464

Deardorff JW (1970) Preliminary results from numerical integrations of unstable planetary boundary layer. J Atmos Sci 27:1209–1211

Dolas PM, Ramchandran R, Sen Gupta K, Patil SM, Jadhav PN (2002) Atmospheric surface-layer processes during the total solar eclipse of 11 August 1999. Boundary-Layer Meteorol 104:445–461

Emanuel KA (1994) Atmospheric convection. Oxford University Press, New York, 580 pp

Fernando HJS (2002) Turbulence in stratified fluids. In: Grimshaw R (ed) Environmental stratified flows, vol III. Kluwer Academic Publishers, Norwell, 296 pp

Girard-Ardhuin F, Benech B, Campistron B, Dessens J, Jacoby-Koaly S (2003) Remote sensing and surface observations of the response of the atmospheric boundary layer to a solar eclipse. Boundary-Layer Meteorol 106:93–115

Goulart A, Degrazia G, Rizza U, Anfossi D (2003) A theoretical model for the study of convective turbulence decay and comparison with large-eddy simulation data. Boundary-Layer Meteorol 107:143–155

Goulart A, Bodmann B, de Vilhena M, Soares P, Moreira D (2010) On the time evolution of the turbulent kinetic energy spectrum for decaying turbulence in the convective boundary layer. Boundary-Layer Meteorol 138:61–75

Grant ALM (1997) An observational study of the evening transition boundary-layer. Q J Roy Meteorol Soc 123:657–677

Higgins CW, Meneveau C, Parlange MB (2007) The effect of filter dimension on the subgrid-scale stress, heat flux, and tensor alignments in the atmospheric surface layer. J Atmos Ocean Technol 24:360–375

Kang HS, Chester S, Meneveau C (2003) Decaying turbulence in an active-grid-generated flow and comparisons with large-eddy simulation. J Fluid Mech 480:129–160

Kleissl J, Kumar V, Meneveau C, Parlange MB (2006) Numerical study of dynamic Smagorinsky models in large-eddy simulation of the atmospheric boundary layer: validation in stable and unstable conditions. Water Resour Res 42:W06D10. doi:10.1029/2005wr004685

Kumar V, Kleissl J, Meneveau C, Parlange MB (2006) Large-eddy simulation of a diurnal cycle of the atmospheric boundary layer: atmospheric stability and scaling issues. Water Resour Res 42:W06D09. doi:10.1029/2005WR004651

Kumar V, Svensson G, Holtslag AAM, Meneveau C, Parlange MB (2010) Impact of surface flux formulations and geostrophic forcing on large-eddy simulations of diurnal atmospheric boundary layer flow. J Appl Meteorol Climatol 49:1496–1516

Metzger M, Holmes H (2008) Time scales in the unstable atmospheric surface layer. Boundary-Layer Meteorol 126:29–50

Nieuwstadt FTM, Brost RA (1986) The decay of convective turbulence. J Atmos Sci 43:532–546

Pardyjak ER (2001) Atmospheric boundary layer dynamics in regions of complex terrain. PhD thesis, Arizona State University

Pardyjak ER, Monti P, Fernando HJS (2002) Flux Richardson number measurements in stable atmospheric shear flows. J Fluid Mech 459:307–316

Pardyjak ER, Fernando HJS, Hunt JCR, Grachev AA, Anderson J (2009) A case study of the development of nocturnal slope flows in a wide open valley and associated air quality implications. Meteorol Z 18:85–100

Pino D, Jonker HJJ, de Arellano JVG, Dosio A (2006) Role of shear and the inversion strength during sunset turbulence over land: characteristic length scales. Boundary-Layer Meteorol 121:537–556

Ramamurthy P, Pardyjak ER (2010) Understanding the behavior of carbon dioxide and surface energy fluxes in the semi-arid Salt Lake Valley Utah USA. Atmos Environ 45:73–84

Sorbjan Z (1997) Decay of convective turbulence revisited. Boundary-Layer Meteorol 82:501–515

Sorbjan Z (2007) A numerical study of daily transitions in the convective boundary layer. Boundary-Layer Meteorol 123:365–383

Strang EJ, Fernando HJS (2001) Entrainment and mixing in stratified shear flows. J Fluid Mech 428:349–386

Stull RB (1988) An introduction to boundary layer meteorology. Kluwer Academic Publishers, The Netherlands, 666 pp

Stull RB (2000) Meteorology for scientists and engineers. Brooks/Cole Thomson, Pacific Grove, 502 pp